Ultrafast Ultrasound Imaging for Micro-Nanomotors: A Phantom Study

Shaoyuan Yan[1], Jinrun Liu[2], Xingyi Guo[1], Dean Ta[1], Gaoshan Huang[2], Alexander A. Solovev[2], Yongfeng Mei[*2], Kailiang Xu[*1]
[1]Center for Biomedical Engineering, Fudan University, Shanghai, China
[2]Department of Materials Science, Fudan University, Shanghai, China

***Abstract*—Recently, micro-nanomotors (MNMs) that effectively convert diverse energy sources into movement and force have received tremendous attention. Due to the ability to be navigated into hard-to-reach tissues in the human body, MNMs have the potential for broad biomedical applications, *e.g.*, targeted drug delivery, cell manipulation, and minimally invasive microsurgeries *etc*. However, despite the great promise, existing imaging technologies are insufficient for imaging and tracking MNMs in deep tissue. To overcome such a limitation, we apply the ultrafast ultrasound method for real-time MNMs imaging in a tissue-mimicking phantom. In addition, advanced detecting, localization and tracking algorithms are used to display the position, trajectory, orientation and velocity of the MNMs. Results of the phantom study demonstrate the feasibility of ultrafast ultrasound imaging as a sufficient technique to image and track MNMs in deep tissue with high spatiotemporal resolution, deep penetration and high sensitivity.**

Keywords—Micro-nanomotors, Ultrafast ultrasound imaging, Clutter filter, Target tracking, Micro-nanorobots.

I. Introduction

MNMs are synthetic micro/nanoscale devices capable of performing self-propelled motion in fluids through converting different types of energies into mechanical movement [1]. With the advantages of active controllable movement, sensitive stimulus-response, multi-function, biocompatibility and massive production [2], MNMs hold great promise toward biomedical applications and have been exploited in microsurgery [3], cellular cargo delivery [4], targeted drug delivery [5], thrombolysis in microvessels [6], etc. For clinical application, it is crucial to explore new imaging method for real time tracking and controlling the MNMs in deep tissue.

Most MNMs experiments have been done using optical microscopy *in vitro*, which neglects the tissue influences for the imaging and cannot be applied for deep MNM imaging [7]. Recently, considerable efforts based on different physical principles have been made to *in-vivo* imaging technologies for MNMs. Fluorescence-based imaging can be applied to observe MNMs in the subcutaneous tissue but it fails in deep organs due to severe attenuation of the light [8]. Both positron emission tomography (PET) and magnetic resonance imaging (MRI) feature excellent tissue-penetration capability and spatial resolution, but have limited temporal resolution and sensitivity [8, 9]. Ultrasound imaging with advantages of non-invasion, safety, deep penetration and low cost, holding bright prospect to complement these existing techniques [10]. However, due to relatively low spatiotemporal resolution, it is challenging to apply the traditional B-mode ultrasound for MNMs imaging [11]. In the last decade, plane wave-based ultrafast ultrasound imaging has been rapidly developed [12, 13]. Compared with the traditional line-by-line focused ultrasound imaging techniques, plane wave imaging can significantly increase the image framerate (up to 10000 frames per second) [14]. To enhance the signal-to-noise ratio (SNR), coherent plane-wave compounding strategy is developed by using ultrafast acquisition consists of multiangle tilted plane waves [15].

In this study, we apply the ultrafast ultrasound for MNMs real-time imaging. Spatiotemporal SVD filter is used to remove clutter signal including tissue signal and noise [16, 17]. The tracking algorithm is implemented based on the Hungarian method for assignment [18]. The feasibility of the proposed methods is demonstrated via phantom experiments on hydrogel micromotors.

II. Materials And Methods

In this section, we introduce the fabrication of the special hydrogel micromotors. In the second subsection, experimental setups including tissue-mimicking phantom and imaging system are presented. The data acquisition and processing of plane-wave ultrasound are detailed in the third subsection. The following subsection is dedicated to the spatiotemporal filtering method based on singular value decomposition (SVD) that uses a frequency-amplitude double thresholds for clutter filtering and MNM extraction. In the last subsection, the principles of localization, tracking and velocity estimation algorithms are presented.

A. Hydrogel Micromotor Preparation

The feasibility of ultrafast ultrasound imaging for MNM is carried out using hydrogel micromotors, which is fabricated using gas core and Fe-plated shell. The micromotors were fabricated using microfluidic technology combining with e-beam deposition technology [19]. Firstly, the mixture of the hydrophobic monomers (methacrylic anhydride and ethylene glycol dimethacrylate) and photoinitiator 2-hydroxy-2-methylpropiophenone was injected in middle phase with a syringe pump as droplet shell, while nitrogen was injected in inner phase as droplet core, and poly vinyl alcohol aqueous was injected in outer phase as dispersion. Micro droplets with a diameter of ~20 μm were generated in mass scale in the microfluidic device. Followed by ultraviolet light exposure, the shell of the droplet cured and the generated microcapsules were collected in a glass petri dish. Secondly, the capsules were treated with pH11 NaOH aqueous for 24 hours to be hydrophilic. Lastly, the collected microcapsules were placed on glass slides and coated with 20 nm Fe layer by e-beam deposition technology.

B. Experiment Setup

As shown in Fig. 1, the tissue-mimicking phantom was an agar block with bifurcated channels inside. The diameter of the channels was about 0.6 mm. Micromotors dispersion was

Project supported by National Natural Science Foundation of China (Grant Nos. 51961145108, 11974081), Natural Science Foundation of Shanghai, China (No. 19ZR1402700), Shanghai Rising Star Program, China (Grant No. 20QC1400200), and Shanghai Academic Research Leader Program, China (No. 19XD1400500).

Corresponding author: Kailiang Xu, xukl@fudan.edu.cn; Yongfeng Mei, yfm@fudan.edu.cn

2021 IEEE International Ultrasonics Symposium (IUS) | 978-1-6654-0355-9/21/$31.00 ©2021 IEEE | DOI: 10.1109/IUS52206.2021.9593877

978-0-7381-1209-1/21/$31.00 ©2021 IEEE

injected into the inlet of a channel at a constant speed by syringe pump, and flowed out from the two outlets. Ultrasound is emitted and acquired with a linear array probe (L11-4v, Verasonics, WA, USA) and a commercial multichannel ultrasound platform (Vantage-256, Verasonics, WA, USA). The probe has 128 transducer elements with a pitch of 0.3 mm and a center frequency of 7.24 MHz with a bandwidth of 6.78 MHz (67%, -6 dB).

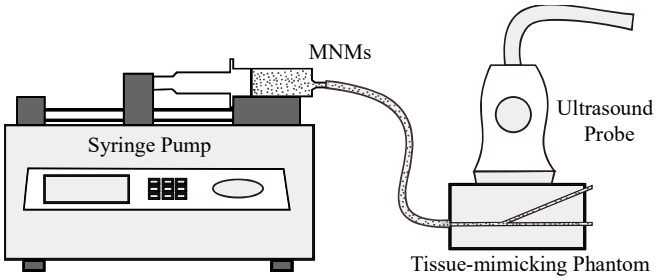

Fig. 1. Experimental setup for ultrafast ultrasound imaging of MNMs in phantom.

C. Acquisition and Processing

To ensure sufficient temporal resolution, ultrafast plane-wave insonification is used. Coherent plane waves are emitted at 7 angles from -10° to 10° at a pulse repetition rate of 2.8 kHz. 14000 radio frequency (RF) echoes are continuously acquired during 5 s. Then RF signals are beamformed using a self-developed GPU-based delay-and-sum algorithm and computed into complex in-phase quadrature (IQ) signals. After coherently compounding IQ signals in angles, high-quality B-mode images are obtained at a 400 Hz framerate. Using the 7.24 MHz ultrasound probe, a large-field 2-D image (3.8 cm× 3 cm) is acquired in the lateral-axial plane.

D. SVD-based Clutter Filtering

Due to tissue clutter having stronger echoes magnitude than MNMs and ultrasonic speckle noise, it is difficult to directly observe the moving MNMs in B-mode images. A spatiotemporal SVD filter is applied to remove tissue clutter signals, and extract the dynamic MNMs images. The ultrafast ultrasonic dataset is represented in the form of a variable $s(x,z,t)$ of size (n_x, n_z, n_t). It is rearranged into a 2-D space-time Casorati matrix S in dimension $(n_{x\times z}, n_t)$ [20]. Then, the SVD of this matrix S is written as

$$S = \sum_k \sigma_k e_k u_k{}^T \tag{1}$$

$$\Rightarrow S^T S = \sum_k \lambda_k e_k e_k{}^T,\ \lambda_k = \sigma_k{}^2 \tag{2}$$

where σ_k is the k th singular value with e_k and u_k as the corresponding left/right singular vectors. The eigenvalue decomposition (EVD) of the square matrix $S^T S$ is computed in (2), where λ_k is the k th eigenvalue, and e_k is the k th eigenvector.

By investigating the frequency content of the individual eigenvectors, Doppler spectrum of each eigen-component can be obtained [21]. The Doppler frequency of the k th eigenvector can be estimated using the lag-one autocorrelation formula as given by [22]

$$f_{D(k)} = \frac{PRF \cdot \arg(R(1)_k)}{2\pi},$$

$$\text{for } R(1)_k = \frac{1}{n_t - 1}\sum_{j=1}^{n_t-1} e_k{}^*(j) e_k(j+1) \tag{3}$$

where PRF means pulse repetition frequency, and $R(1)_k$ represents the lag-one autocorrelation value for the k th eigenvector.

From the frequency and energy perspective, tissue echoes correspond to low Doppler frequency with large magnitude eigen-components. With the amplitude of the eigenvalues and the frequency estimates, the tissue clutter eigen-components can thus be filtered out using two thresholds, *i.e.*, frequency threshold f_0 and amplitude threshold A_0. In the study, the thresholds of f_0 and A_0 are selected empirically. The resulting tissue clutter eigen-component set ϕ_c can be represented as:

$$\phi_c = \left\{ e_k \middle| (f_{D(k)} < f_0) \,\&\, (\lambda_k > A_0) \right\} \tag{4}$$

After setting the eigenvalues corresponding to ϕ_c to zero, the clutter filtered ultrasonic data S_f can be derived after substituting λ_k' into (2). Rearrange the 2-D matrix S_f into a 3-D matrix s_f in dimension (n_x, n_z, n_t), and the clutter filtered images of the hydrogel micromotors can thus be obtained.

E. Power Doppler Imaging

After clutter filtering, power Doppler images can be computed by

$$PD(x,z) = \frac{1}{n_t}\sum_{t=1}^{n_t} \left| s_f(x,z,t) \right|^2 \tag{5}$$

The power in each sub-pixel is proportional to and can be used to quantify the number of MNMs passing through [23].

F. Localization、Tracking and Velocity Estimation

After clutter filtering, the backscattering amplitude of the gas-filled MNM is typically higher than the background. A fast and efficient localization strategy is applied to find regional maxima in each frame. Thanks to the high-framerate imaging, an MNM in the current frame is most likely to be the closest one in the next frame. Therefore, the targets can be robustly tracked by pairing targets between consecutive frames in a bipartite graph fashion to minimize total pairing distance [24]. Hungarian algorithm, already exploited in transportation analysis [25], is used here to pair MNMs between consecutive frames. The pairing distance and direction are recorded to track MNM movement from frame to frame. The velocity vector map can thus be obtained after MNMs localization.

III. Results

Figure 2 shows the optical image of the hydrogel micromotors used in the experiment. A frame of compounded B-mode image and clutter filtered image are displayed in Figs. 3(a) and (b), respectively. As shown in Fig. 3(a), it is difficult to observe MNMs directly due to the low contrast between MNMs and tissue. However, after tissue clutter filtering, MNMs can be visualized clearly.

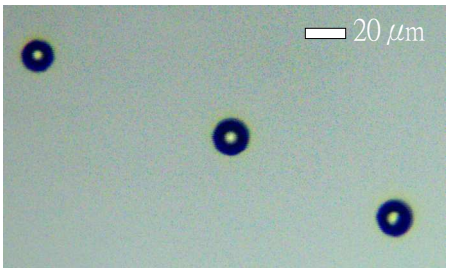

Fig. 2. Optical image of the hydrogel micromotors.

Perform SVD on a dataset of 2000 compounded images acquired within 5 seconds according to (1). The eigenvalues are arranged in a descending order. Normalized eigenvalues are plotted in dB in Fig. 4(a). Fig. 4(b) shows the principle of eigen-components selection. The X-axis and Y-axis are normalized eigenvalue and Doppler frequency, respectively. The Eigen-components whose normalized Doppler frequency is smaller than the frequency threshold f_0 and eigenvalue exceeds the amplitude threshold A_0 are selected and set to zero.

Power Doppler images of the MNMs are shown in Fig. 5(a). The phenomenon that more MNMs flowed through the lower branch than the upper branch can be reflected from the power distribution in the power Doppler image. After localization and tracking, a total of 551 tracks are captured within 2000 frames. From the velocity vector map shown in Fig. 5(b), it can be seen the speed of MNMs movement is approximately between 50 ~ 200 mm/s. By averaging the speed of all trajectories, the average speed is around 113.7 mm/s.

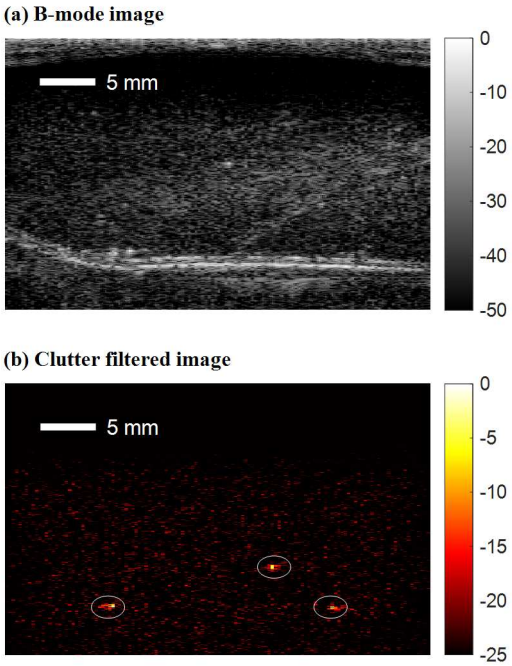

Fig. 3. Ultrafast ultrasound imaging of MNMs, (a) DAS beamformed and coherently compounded B-mode image of MNMs in tissue-mimicking phantom; (b) clutter filtered image based on SVD. MNMs are highlighted by white circles.

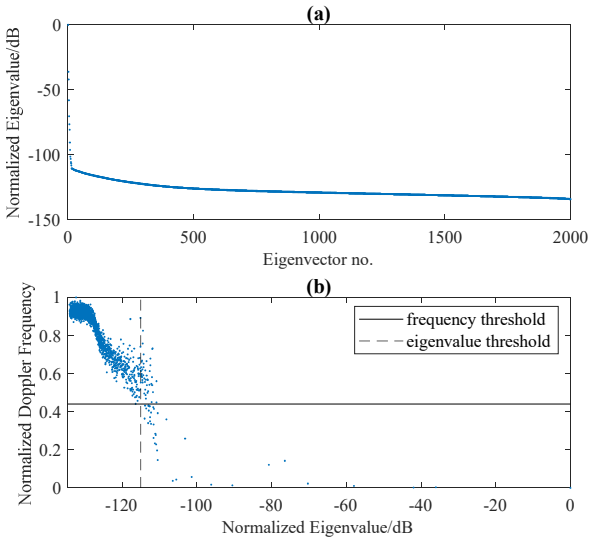

Fig. 4. SVD and Doppler frequency analysis results, (a) normalized eigenvalues; (b) normalized eigenvalues versus normalized Doppler frequency.

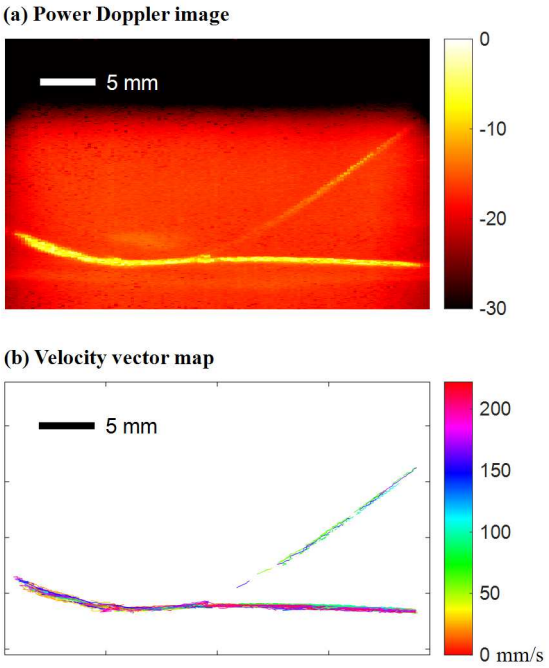

Fig. 5. Experimental results of ultrafast ultrasound MNMs imaging and tracking, (a) power Doppler images; (b) velocity vector map of the MNM trajectories.

IV. Discussion

In this work, plane wave-based ultrafast ultrasound imaging method is used to detect MNMs. Thanks to the high framerate (2800 frames per second), the sensitivity of ultrasound imaging is sufficient to detect tiny and moving MNMs. As shown in the experimental results, the spatiotemporal SVD clutter filter can remove the tissue clutter signals efficiently. In addition to the eigenvalue, Doppler frequency parameter is proposed for eigen-component selection, which can achieve better filtering results. Furthermore, the power Doppler image can reflect the degree of enrichment of the MNMs in different positions.

Regional maxima searching is a straightforward method to locate the MNMs in the clutter filtered image. However, the disadvantage is that we need to set an appropriate threshold manually according to the typical magnitude of the MNMs. Inappropriate threshold selection may result in microbubbles omission or incorrect positioning. Convolving the filtered image with the point spread function can achieve a better localization [26].

The velocity of MNMs is determined from positions in a 2-D plane. However, MNMs may enter and leave the image section and change their direction in 3-D, leading to inaccurate velocity estimation. 3-D imaging and tracking can be considered in future study.

V. Conclusion

We perform the ultrafast ultrasound imaging for real-time MNM imaging and tracking in a tissue-mimicking phantom. Experiments demonstrate that MNMs are detectable after high framerate acquisition and clutter filter. The distribution of MNMs can also be obtained in the power Doppler image. After localizing the position of MNMs in each frame, the trajectories and velocity vector map can be obtained by using the super-resolution ultrasonic localization microscopy. To conclude, we propose a new approach of real-time imaging and tracking MNMs in deep tissue, which paves the way for the *in vivo* application of MNMs under the ultrasound imaging guidance.

References

[1] W. Wang, W. Duan, S. Ahmed, T. E. Mallouk, and A. Sen, "Small power: Autonomous nano- and micromotors propelled by self-generated gradients," Nano Today, vol. 8, no. 5, pp. 531-554, 2013.

[2] X. Lin, Z. Wu, Y. Wu, M. Xuan, and Q. He, "Self-propelled micro-/nanomotors based on controlled assembled architectures," Adv Mater, vol. 28, no. 6, pp. 1060-72, 2016.

[3] L. Zhang, J. J. Abbott, L. Dong, B. E. Kratochvil, D. Bell, and B. J. Nelson, "Artificial bacterial flagella: Fabrication and magnetic control," Applied Physics Letters, vol. 94, no. 6, pp. 064107, 2009.

[4] M. Medina-Sanchez, L. Schwarz, A. K. Meyer, F. Hebenstreit, and O. G. Schmidt, "Cellular cargo delivery: Toward assisted fertilization by sperm-carrying micromotors," Nano Lett, vol. 16, no. 1, pp. 555-61, 2016.

[5] C. M. Hu, R. H. Fang, J. Copp, B. T. Luk, and L. Zhang, "A biomimetic nanosponge that absorbs pore-forming toxins," Nat Nanotechnol, vol. 8, no. 5, pp. 336-40, 2013.

[6] R. Cheng, W. Huang, L. Huang, B. Yang, L. Mao, K. Jin, Q. ZhuGe, and Y. Zhao, "Acceleration of tissue plasminogen activator-mediated thrombolysis by magnetically powered nanomotors," ACS Nano, vol. 8, no. 8, pp. 7746-7754, 2014.

[7] M. Medina-Sánchez, and O. G. Schmidt, "Medical microbots need better imaging and control," Nature, vol. 545, no. 7655, pp. 406-408, 2017.

[8] X. Yan, Q. Zhou, M. Vincent, Y. Deng, J. Yu, J. Xu, T. Xu, T. Tang, L. Bian, Y.-X. J. Wang, K. Kostarelos, and L. Zhang, "Multifunctional biohybrid magnetite microrobots for imaging-guided therapy," Science Robotics, vol. 2, no. 12, pp. eaaq1155, 2017.

[9] D. Vilela, U. Cossío, J. Parmar, A. M. Martínez-Villacorta, V. Gómez-Vallejo, J. Llop, and S. Sánchez, "Medical imaging for the tracking of micromotors," ACS Nano, vol. 12, no. 2, pp. 1220-1227, 2018.

[10] M. Imbault, D. Chauvet, J. L. Gennisson, L. Capelle, and M. Tanter, "Intraoperative functional ultrasound imaging of human brain activity," Sci Rep, vol. 7, no. 1, pp. 7304, 2017.

[11] S. Pane, V. Iacovacci, E. Sinibaldi, and A. Menciassi, "Real-time imaging and tracking of microrobots in tissues using ultrasound phase analysis," Applied Physics Letters, vol. 118, no. 1, pp. 14102, 2021.

[12] D. Garcia, L. Le Tarnec, S. Muth, E. Montagnon, J. Poree, and G. Cloutier, "Stolt's f-k migration for plane wave ultrasound imaging," IEEE Trans Ultrason Ferroelectr Freq Control, vol. 60, no. 9, pp. 1853-67, 2013.

[13] M. Correia, J. Provost, M. Tanter, and M. Pernot, "4D ultrafast ultrasound flow imaging: in vivo quantification of arterial volumetric flow rate in a single heartbeat," Phys Med Biol, vol. 61, no. 23, pp. L48-L61, 2016.

[14] M. Tanter, and M. Fink, "Ultrafast imaging in biomedical ultrasound," IEEE Trans Ultrason Ferroelectr Freq Control, vol. 61, no. 1, pp. 102-119, 2014.

[15] G. Montaldo, M. Tanter, J. Bercoff, N. Benech, and M. Fink, "Coherent plane-wave compounding for very high frame rate ultrasonography and transient elastography," IEEE Trans Ultrason Ferroelectr Freq Control, vol. 56, no. 3, pp. 489-506, 2009.

[16] C. Demene, T. Deffieux, M. Pernot, B. F. Osmanski, V. Biran, J. L. Gennisson, L. A. Sieu, A. Bergel, S. Franqui, J. M. Correas, I. Cohen, O. Baud, and M. Tanter, "Spatiotemporal clutter filtering of ultrafast ultrasound data highly increases Doppler and fultrasound sensitivity," IEEE Trans Med Imaging, vol. 34, no. 11, pp. 2271-85, 2015.

[17] J. Zang, K. Xu, Q. Han, Q. Lu, Y. Mei and D. Ta, "Non-contrast-enhanced ultrafast ultrasound Doppler imaging of spinal cord micro-vessels, "Acta Physica Sinica, vol. 70, no. 11, pp. 114304-1, 2021.

[18] B. Heiles, M. Correia, V. Hingot, M. Pernot, J. Provost, M. Tanter, and O. Couture, "Ultrafast 3D ultrasound localization microscopy using a 32 x 32 matrix array," IEEE Trans Med Imaging, vol. 38, no. 9, pp. 2005-2015, 2019.

[19] H. Zhu, S. Nawar, J. G. Werner, J. Liu, G. Huang, Y. Mei, D. A. Weitz, and A. A. Solovev, "Hydrogel micromotors with catalyst-containing liquid core and shell," J Phys Condens Matter, vol. 31, no. 21, pp. 214004, 2019.

[20] E. J. Candes, C. A. Sing-Long, and J. D. Trzasko, "Unbiased risk estimates for singular value thresholding and spectral estimators," IEEE Trans Sig Processing, vol. 61, no. 19, pp. 4643-4657, 2013.

[21] C. H. Alfred and L. Lovstakken, "Eigen-based clutter filter design for ultrasound color flow imaging: A review," IEEE Trans Ultrason Ferroelectr Freq Control, vol. 57, no.5, pp. 1096-1111, 2010.

[22] C. Kasai, K. Namekawa, A. Koyano, and R. Omoto, "Real-time two-dimensional blood flow imaging using an autocorrelation technique," IEEE Trans Sonics and Ultrasonics, vol. 32, no. 3, pp. 458-464, 1985.

[23] T. Deffieux, C. Demene, and M. Tanter, "Functional ultrasound imaging: A new imaging modality for neuroscience," Neuroscience, pp. 0306-4522, 2021.

[24] S. Jonas, D. Bhattacharya, M. K. Khokha, and M. A. Choma, "Microfluidic characterization of cilia-driven fluid flow using optical coherence tomography-based particle tracking velocimetry," Biomedical Optics Express, vol. 2, no. 7, pp. 2022-2034, 2011.

[25] H. W. Kuhn, "The Hungarian method for the assignment problem," in Naval Research Logistics Quarterly, Hoboken, NJ, USA:Wiley Online Library, 1995.

[26] D. Ackermann, and G. Schmitz, "Detection and tracking of multiple microbubbles in ultrasound b-mode images," IEEE Trans Ultrason Ferroelectr Freq Control, vol. 63, no. 1, pp. 72-82, 2016.